Probing helix formation in chains of vertex-linked octahedra†‡

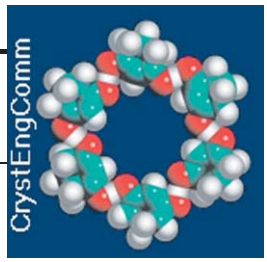

Highlight

Paul A. Maggard,[a] Amy L. Kopf,[b] Charlotte L. Stern[b] and Kenneth R. Poeppelmeier*[b]

[a]*Department of Chemistry, 2620 Yarbrough Drive, North Carolina State University, Raleigh, NC 27695-8204, USA*
[b]*Department of Chemistry, 2145 Sheridan Road, Northwestern University, Evanston, IL 60208-3113, USA. E-mail: krp@northwestern.edu*

Received 4th May 2004, Accepted 22nd June 2004
First published as an Advance Article on the web 17th September 2004

The rational design of crystal structures based on the chemical nature of molecular components, a longstanding and exciting research topic in organic solid state chemistry, is an emerging theme of crystal engineering in inorganic solid state chemistry. In particular, noncentrosymmetric structures, or those lacking inversion symmetry, are important for future technologies that are based on piezoelectricity, pyroelectricity, ferroelectricity and second harmonic generation (SHG). Materials that exhibit these properties provide a large and new class of solids for studies in basic science associated with the noncentrosymmetric (chiral, polar, or chiral–polar) space groups. Structures comprised of vertex-linked octahedra are common in inorganic solids. The subject of our Highlight is the rational synthesis of linear, zigzag or helical chains when two vertices of an octahedron, which are either adjacent (*cis*) or opposite (*trans*), are linked.

† Based on the presentation given at CrystEngComm Discussion: New Trends in Crystal Engineering, 8–10 September 2004, Nottingham, UK.
‡ Electronic supplementary information (ESI) available: Mid-infrared spectrum and SQUID spectrum. See http://www.rsc.org/suppdata/ce/b4/b406621a/

Introduction

The fields of structural inorganic and organic chemistry have grown enormously over the past several years. The design of new structural topologies and the elucidation of structural

Paul A. Maggard obtained his Ph.D. from Iowa State University, Ames, Iowa in 2000. Subsequently, he took a postdoctoral fellowship at Northwestern University, Evanston, Illinois, working with K. R. Poeppelmeier (2000–2002). He is currently an Assistant Professor of Inorganic Chemistry at North Carolina State University, Raleigh, North Carolina. His major research emphasis is on the synthesis and characterization of novel transition metal oxides and transition metal silicides. He is the recipient of the 2004 Arnold and Mabel Beckman Foundation Young Investigator Award.

Amy L. Kopf received her B.Sc. in Chemistry from Michigan State University, East Lansing, Michigan in 1999. Under the supervision of Prof. Joan B. Broderick, her research focus was the biosynthesis of iron–sulfur clusters, particularly the $[3Fe–4S]^{+}$ cluster, found in Pyruvate Formate-Lyase Activating Enzyme under anaerobic isolation. She is currently a graduate student at Northwestern University, Evanston, Illinois in the laboratory of Prof. Kenneth R. Poeppelmeier. Her thesis research project is using hydrothermal synthesis methods for crystal growth of mixed metal oxide and oxide/fluoride compounds.

Charlotte L. Stern earned her B.Sc. in Chemistry from the University of Illinois at Urbana-Champaign, Illinois in 1986. After graduation until 1990, she was the staff crystallographer at the University of Illinois at Urbana-Champaign. She then came to Northwestern University as the Chemistry Department crystallographer. Her work has included data collection and structure determination for organic, inorganic, and organometallic materials. She has over 250 publications and collaborates with numerous research groups.

Kenneth R. Poeppelmeier obtained his Ph.D. in 1978 from Iowa State University, Ames, Iowa. From 1978 to 1984 he pursued research in the area of solid state chemistry at the Exxon Research and Engineering Company in Annandale, New Jersey. Since 1984 he has been a member of the faculty at Northwestern University Department of Chemistry, Evanston, Illinois. His interests at Northwestern University have included the synthesis of mixed metal and thin film oxides, preparation of single crystals, X-ray, neutron and electron diffraction. He has authored over 230 publications and 11 patents.


Paul A. Maggard


Amy L. Kopf


Charlotte L. Stern


Kenneth R. Poeppelmeier

design principles have served to increase the chemist's control over the properties of solid-state structures.[1,2] It is well known that noncentrosymmetric solids, *i.e.* those with no centers of symmetry, give rise to important dielectric and elastic properties, including ferro-, pyro- or piezoelectricity, ferroelasticity and optical activity.[3,4] While the particular (noncentrosymmetric) crystal classes required for solids to exhibit these properties have been mathematically derived and are well known,[5] the structural design principles that facilitate supramolecular assembly of polar, chiral or polar–chiral structures must be understood in order for the chemist to project particular molecular or ionic chemical species, inorganic as well as organic, into the appropriate crystal classes.

Owing to their chirality, helices play a prominent role in many noncentrosymmetric solids. Helical chains are important in biological systems and are found at many length scales, ranging from DNA to proteins and small peptide chains. α-Helices are found in nearly all globular proteins. The α -helix is primarily stabilized by hydrogen bonds between backbone amide groups.[6] Biophysicists have been able to manipulate the helical content in short peptides *via* a *trans*-to-*cis* photoisomerization using an azobenzene cross-linker.[7] Another method of favoring a helical chain in a short peptide is through the use of bulky side chains; the ideology has been supported by work in the gas phase by Jarrold, *et al.*[8,9] These few examples serve to highlight the manipulation of the helix conformation in biological systems.

Although numerous mixed inorganic–organic chain structures have been identified and are well characterized, few comparative studies have been reported that reveal why chain structures adopt chiral symmetries. Still fewer studies have focused on polar symmetries, despite reports of many chain-forming materials which belong to families of compositionally-similar solids. Some recent examples of helical and polar chain structures include the infinite chains of edge-sharing ZrF_6^{2-} antiprisms in the newly-discovered ferroelectric aminoguanidinium(2+)hexafluorozirconate ($CN_4H_8ZrF_6$),[10] the mixed-metal polar chains in $Cu(C_5H_5N)_4Cr_2O_7$ (C_5H_5N = pyridine, py) and $(Ag_3MoO_3F_3)(Ag_3MoO_4)Cl$,[11,12] the helical $[(VO_2)(HPO_4)]_\infty$ chains in $M(C_{10}H_{10}N)_2(VO_2)_2(HPO_4)_4$ (M = Co, Ni, $C_{10}H_{10}N$ = 4,4′-bipyridine, 4,4′-bpy),[13] the infinite 2_1 helical polymers (of both chiralities) in $[Ag(C_4H_4N_2)](NO_3)$ ($C_4H_4N_2$ = pyridazine, pydz),[14] and the helical metal-oxide/fluoride chains reported in $M(C_4H_4N_2)(H_2O)_2MoO_2F_4$ (M = Zn, Cd, $C_4H_4N_2$ = pyrazine, pyz).[15]

In recent years, our research has focused on the problem of how to crystallize the well known acentric metal oxide/fluoride species MOF_5^{2-} (M = V, Nb, Ta) and $MO_2F_4^{2-}$ (M = Mo, W) in noncentrosymmetric and, ideally, polar structures. Among the over 30 solid-state structures reported for the metal oxide/fluoride systems containing MX_6^{2-} anions (M = Ti, Zr, V, Nb, Ta, Mo, W; X = O, F) and $M'L_4^{2+}$ cations (M′ = Cu, Zn, Cd; L = H_2O or N-containing ligand), several common structural design principles have emerged. The first strategies implemented to begin to target noncentrosymmetric structures, which are comprised of these acentric octahedra and where local ordering of the oxide/fluoride ligands is required, were focused on using appropriate hydrogen-bonding ligands, as in $[HNC_6H_6OH]_2[Cu(py)_4(WO_2F_4)_2]$,[16] or coordination by multiple cation types in $[pyH]_2[Cu(py)_4(MX_6)_2]$ (MX_6 = ZrF_6^{2-}, $NbOF_5^{2-}$, $MoO_2F_4^{2-}$).[17] Another general structural principle is evident in the example of $M(pyz)(H_2O)_2MoO_2F_4$ (M = Zn, Cd),[15,18] where close-packed helical chains linked by pyrazine lead to the formation of a 3D chiral structure. Three distinct chain geometries are observed that can be thought of as a progression from a linear to a bent or zigzag to a helical chain. This is illustrated in Fig. 1. As in all solid-state systems, the large number of possible packing of atoms, clusters, and sheets continues to hamper attempts to predict additional compositions with a desired topology (*e.g.*, helical chains), including the simple interchange of related elements of the solid.

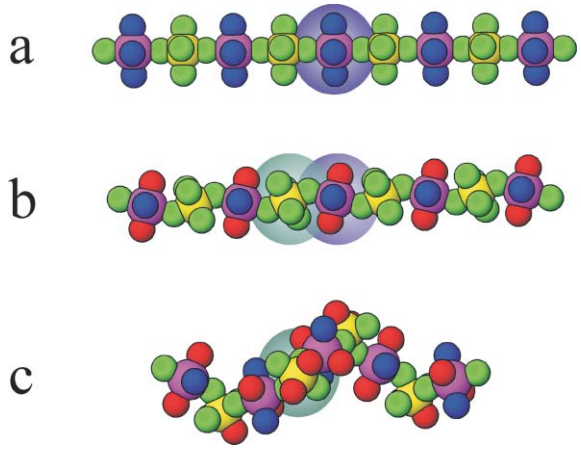

Fig. 1 The progression of a linear chain as in (a) $Cu(py)_4MX_6$ (M = TiF_6^{2-}, ZrF_6^{2-}, HfF_6^{2-}, $NbOF_5^{2-}$, $TaOF_5^{2-}$, $WO_2F_4^{2-}$; py = pyridine) to a zigzag chain in (b) $Cu(py)_2(H_2O)_2WO_2F_4$, and $Cu(pyz)(H_2O)_2TiF_6$ (pyz = pyrazine) to a helical chain in (c) $M(pyz)(H_2O)_2MoO_2F_4$ (M = Zn, Cd). The cation and anion octahedra are highlighted with purple and blue shadings, respectively.

"An indefinitely large number" of inorganic structures are derived from vertex-linked octahedra.[19] In this Highlight we focus on a series of systematic chemical modifications to cationic $M'L_4^{2+}$ and anionic $MO_xF_{6-x}^{2-}$ fragments in order to understand the factors that lead to helix formation. In $Cu(pyz)(H_2O)_2TiF_6$, for example, alternating *trans*-fluoride, *trans*-vertex-connected $Cu(pyz)_{2/2}(H_2O)_2F_{2/2}$ and $TiF_4F_{2/2}$ octahedra form zigzag chains which join to six neighboring chains, two by Cu–pyz–Cu bridges and four by Cu–O–H···F–Ti contacts. These chains of *trans–trans* vertex-linked octahedra minimize intra-chain repulsion between pyrazine groups, whereas intra-chain repulsion between pyrazine groups assists the formation of helical chains when vertex-linked octahedra are in a *cis–trans* pattern.[18]

Recent experimental results

Caution

Hydrofluoric acid is toxic and corrosive!

Materials

TiO_2 (99.99+%, Aldrich), CuO (99.99+%, Aldrich), pyrazine (99+%, Aldrich) and HF (aqueous, 49% Aldrich) were used as received. Reagent amounts of deionized water were also used in the synthesis.

Synthesis

The synthesis of $Cu(pyz)(H_2O)_2TiF_6$ was performed by adding 8.70×10^{-2} g (1.09×10^{-3} mol) of TiO_2, 8.66×10^{-2} g (1.09×10^{-3} mol) of CuO, 1.74×10^{-1} g (2.18×10^{-3} mol) of pyrazine, 1.564 g (4.41×10^{-2} mol) of 49% aqueous HF and 8.82×10^{-2} g (4.90×10^{-3} mol) of H_2O to a Teflon (fluoro–ethylene–propylene) pouch.[20] The pouches were heat sealed and placed inside a 125 mL Teflon-lined stainless steel reaction vessel which was backfilled with *ca.* 42 mL deionized H_2O before closing. The reaction vessel was heated to 150 °C for 24 h inside a convection oven and slowly cooled to room temperature at 6 °C h^{-1}. Green crystals of $Cu(pyz)(H_2O)_2TiF_6$ were recovered by filtration in *ca.* 78% yield based on Cu, with the remaining amount presumably left in solution. An X-ray powder pattern revealed 100% of the product was the target compound, as judged by a theoretical pattern generated from the single crystal structure solution.

Table 1 Selected atomic coordinates and equivalent isotropic displacement parameters ($Å^2 \times 10^3$) for $Cu(C_4H_4N_2)(H_2O)_2TiF_6$.

Atom	Wyckoff symbol	*x*	*y*	*z*	*U*(eq)[a]
Cu	4e	0.5	0.26929(6)	0.25	0.0118(2)
Ti	4c	0.25	0.25	0.0	0.0108(2)
F1	8f	0.3925(1)	0.2685(2)	0.0605(2)	0.0171(4)
F2	8f	0.2218(2)	0.4703(3)	0.0883(2)	0.0396(6)
F3	8f	0.2255(2)	0.0980(3)	0.1356(2)	0.0367(5)
O[b]	8f	0.6210(2)	0.2749(3)	0.1523(2)	0.0192(4)
N1	4e	0.5	−0.0288(5)	0.25	0.0138(6)
N2	4e	0.5	0.5667(5)	0.25	0.0126(6)
C1[b]	8f	0.4609(2)	0.6683(4)	0.1506(2)	0.0161(5)
C2[b]	8f	0.4607(2)	−0.1301(4)	0.1504(2)	0.0163(5)

[a] *U*(eq) is defined as one-third of the trace of the orthogonalized U_{ij} tensor. [b] Hydrogen atoms were constrained to ride on the parent oxygen and carbon atoms in idealized positions.

Crystallographic structure determination

Several rectangular platelet-shaped crystals were examined under an optical microscope equipped with cross polarizers, and the best were selected for data collection on a Bruker CCD diffractometer operating at 153 K.[21] The unit cell obtained was monoclinic with $a = 12.703(2)$ Å, $b = 6.879(1)$ Å, $c = 10.819(2)$ Å, and $\beta = 95.426(2)^\circ$. One sphere of reflections ($\pm h$, $\pm k$, $\pm l$) was collected and then processed with SAINTPLUS[22] to $2\theta = 56.5^\circ$ to give 4141 reflections, of which 1020 were unique and $F > 2\sigma_F$. The structure was solved and refined using SHELXTL[23] in the monoclinic space group *C*2/*c* (No. 15) and checked for additional symmetry elements using the program PLATON.[24] The final structure refinement included hydrogen atoms on the pyrazine molecules in idealized positions around the ring at a C–H distance of 0.95 Å, and hydrogen atoms on the H_2O molecules in idealized positions at a O–H distance of 0.82 Å. Final anisotropic structure refinement converged at $R1/wR2 = 0.034/0.086$, with a data:variable ratio of 14.8. Selected atomic coordinates and isotropic-equivalent displacement parameters are listed in Table 1. Interatomic contacts for selected bonds are given in Table 2. Included in the supporting information is a complete list of data collection, refinement and anisotropic displacement parameters and all near-neighbor interatomic distances.

CCDC reference number 237769.

See http://www.rsc.org/suppdata/ce/b4/b406621a/ for the crystallographic data, in CIF format.

Spectroscopic measurements

Mid-infrared (400–4000 cm^{-1}) spectra were collected on $Cu(pyz)(H_2O)_2TiF_6$ with a Bio-Rad FTS-60 FTIR spectrophotometer operating at a resolution of 2 cm^{-1}. Both samples were ground and pelletized with dried KBr, transferred to the FTIR, and the FTIR chamber evacuated for 2–5 min before spectra acquisition. Electronic supplementary information (ESI) available: mid-infrared spectrum.‡

Table 2 Selected interatomic distances (Å) and angles (°) in $Cu(C_4H_4N_2)(H_2O)_2TiF_6$.

Atom 1	Atom 2	Mult.	Distance	Intra-polyhedral angles	
Ti	F1	2×	1.870(2)		
	F2	2×	1.844(2)		
	F3	2×	1.852(2)	TiF_6^{2-}octahedron	
				F1–Ti–F2	89.52(8)
Cu	O1	2×	1.947(2)	F1–Ti–F2	90.48(8)
	F1	2×	2.353(2)	F1–Ti–F3	89.46(8)
	N1		2.051(3)	F1–Ti–F3	90.54(8)
	N2		2.046(3)	F2–Ti–F3	89.9(1)
				F2–Ti–F3	90.1(1)
N1	C2	2×	1.339(3)		
N2	C1	2×	1.338(3)		
C1	C2		1.387(4)		

Magnetic susceptibility

A pure polycrystalline sample of $Cu(pyz)(H_2O)_2TiF_6$ was loaded and sealed into gelatin capsules and the magnetization measured from 5 to 300 K at a field of 1 kG with a Quantum Design Corp. MPMS SQUID. The data were corrected for the diamagnetism of the sample holder and atomic cores.[25] Electronic supplementary information (ESI) available: SQUID spectrum.‡

Results and discussion

Structural description

The crystal structure of $Cu(pyz)(H_2O)_2TiF_6$, viewed down *ca.* [101] (*b*-axis is horizontal), is illustrated in Fig. 2 and the corresponding symmetry inequivalent bonds are listed in Table 2. The structure is comprised of one symmetry unique chain, which is projected into the plane of the page, that has a repeating [–Cu–F–Ti–F–] zigzag backbone. Each chain has covalent Cu–pyz–Cu bridges to two neighboring chains (Cu–N at 2.051(3) and 2.04693 Å) and Cu–OH···F–Ti hydrogen bonds to four other chains (OH···F at 1.78–1.80 Å; unrefined). A total of six interchain bonds are made per $Cu(pyz)_{2/2}(H_2O)_2^{2+}$–$TiF_6^{2-}$ repeat unit, two *via* the bidentate pyrazine bridge and four *via* the hydrogen bond contacts, to form the 3D framework. Consideration of the covalent Cu–pyrazine–TiF_6 network (Fig. 3), however, reveals 2D square nets that stack in an offset arrangement to form hydrogen bond contacts both above and below, as shown in Fig. 2. Relatively large rectangular cavities occur within a single 2D square net (shown in Fig. 3), at *ca.* 4.3 × 6.0 Å, with the coordinated H_2O molecules extending above and below each layer.

The local bonding environment of the titanium (Ti^{4+}) is a

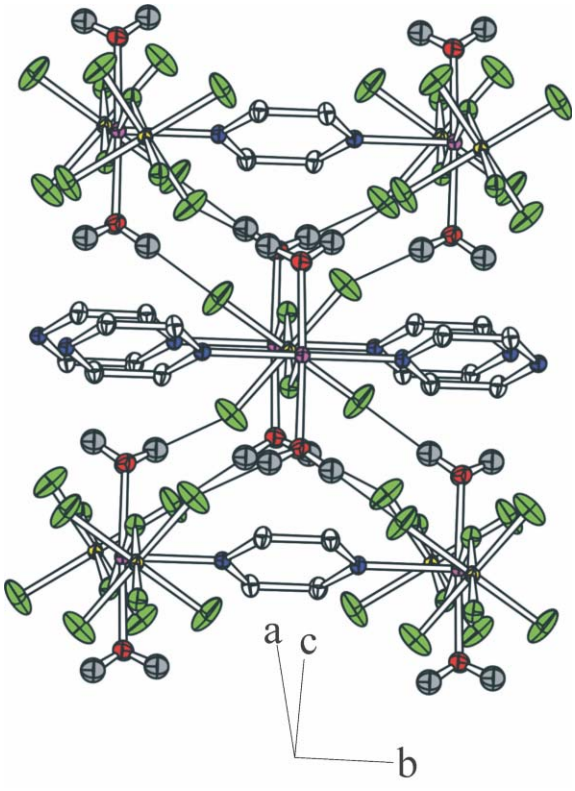

Fig. 2 Structural view of $Cu(pyz)(H_2O)_2TiF_6$ with 50% probability ellipsoids and thin lines for hydrogen bonds. Cu: magenta, Ti: yellow, F: green, O: red, N: blue, C: white, H: grey.

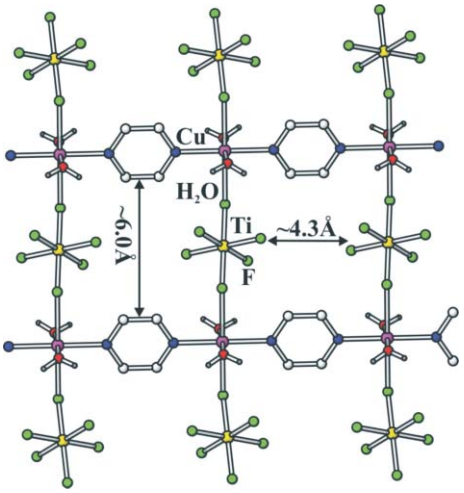

Fig. 3 A ~ [010] view of one $Cu(pyz)(H_2O)_2TiF_6$ layer. Hydrogen bonds to F atoms in neighboring layers extend above and below the plane. Click here to access a 3D view of Fig. 3.

slightly distorted octahedron that closely resembles those of Ti^{4+} ions described in other related structures. A list of selected interatomic distances and angles of $Cu(pyz)(H_2O)_2TiF_6$ is given in Table 2. The titanium atom is surrounded by six almost equidistant fluorine atoms, at 1.844(2)–1.870(2) Å, and is located on an inversion center. Because the titanium atom resides on an inversion site, the Ti–F bonds are symmetric and there is no local dipole moment, unlike what is often observed for ZrF_6^{2-} and the oxide/fluoride anions of the d^0 transition metals.[4,17] The TiF_6^{2-} octahedra are linked through *trans*-fluoride ions to neighboring copper (Cu^{2+}) atoms (Fig. 3) to form the [–Cu–F–Ti–F–] backbone. Furthermore, at 140.16(9)°, the Cu–F–Ti angle is bent as is common for other alternating early and late transition metal chain structures.[15,26] The significance of this bent angle will be discussed in greater detail below. The local octahedral coordination of the Cu^{2+} ion is Jahn–Teller distorted, as expected for a d^9 metal ion, with two longer bonds to the axial fluorine atoms [2.353(2) Å] and four shorter bonds to equatorial H_2O molecules [1.947(2) Å × 2; *trans*] and the nitrogen atoms [2.051(3) and 2.046(3) Å] of the pyrazine ligands. Bond angles around the Cu^{2+}-centered octahedra are nearly regular, and range from 87.13(6)° to 92.88(8)°.

Infrared spectroscopy and magnetic measurements

The observed infrared absorption bands were matched, using standard IR libraries of known compounds,[27,28] with the number of types of bonds and elements present in the structure. A strong and broad IR absorption peak was observed at 3205 cm^{-1} for O–H stretches (hydrogen bonded), and several strong absorption peaks for the pyrazine ligand were present at 1695, 1626, 1417, 1426, 1060–1160, and 800–840 cm^{-1}, corresponding to the various C=C, C–H, and C–C groups. Corresponding to the Ti–F stretches, a large broad peak is observed at *ca.* 563 and 491 cm^{-1}. All of the Cu–L (L = F, OH_2, NC_4H_4N) absorption bands are present at lower energies and were not located in the detectable range of frequencies. After considering diamagnetic corrections for the sample holder and closed-shell atomic cores, green crystals of the solid had a temperature-dependent magnetism that could be fit using the Curie–Weiss Law $\chi = C/(T - \theta)$, with a θ of −9.4 K. A plot of $1/\chi$ *vs.* temperature was linear, with a slope that corresponded to a μ_{eff} of 1.9 BM ($=2.828 \times [\chi(T - \theta)]^{1/2}$), compared to the theoretically calculated 1.73 BM for Cu^{2+} with a spin only contribution of S = ½.[29]

Chains of *trans–trans vs. cis-trans* vertex-linked octahedral

The new structure described above features alternating *trans*-vertex-connected $Cu(pyz)_{2/2}(H_2O)_2F_{2/2}$ and $TiF_4F_{2/2}$ octahedra linked through bent fluoride bridges that generate a zigzag chain and, ultimately, a centrosymmetric structure. This zigzag chain has been described previously as an intermediate structure of a stepwise sequence that features a linear chain, in $Cu(py)_4MX_6$ ($MX_6 = TiF_6^{2-}$, ZrF_6^{2-}, HfF_6^{2-}, $NbOF_5^{2-}$, $TaOF_5^{2-}$, $WO_2F_4^{2-}$; py = pyridine),[30–31] to a zigzag chain (in the title compound and in $Cu(py)_2(H_2O)_2WO_2F_4$),[30] and finally to a helical chain, in $M(pyz)(H_2O)_2MoO_2F_4$ (M = Zn, Cd).[15,18] Each chain type is shown in Fig. 1, where the stepwise sequence is illustrated by the linear (Fig. 1a), zigzag (Fig. 1b) and helical chains (Fig. 1c). The helical chain was the final step towards generating a noncentrosymmetric and chiral solid-state structure (as verified by its SHG-active optical properties) beginning with noncentrosymmetric metal-oxide/fluoride octahedra. The first sequential step, from a linear to zigzag chain, involved a bending of the fluoride bridge between the alternating early/late transition metal ions. This result was achieved by the substitution of H_2O for the organic ligand and the introduction of hydrogen bonding. The second step, from a zigzag to helical chain, was roughly described as arising from the intrachain substitution of a *cis*-directing anion in the chain ($MoO_2F_4^{2-}$) for the *trans*-directing anions (such as TiF_6^{2-}). Other solids comprised of helical chains, such as $KTiOPO_4$,[11,32] feature this *cis–trans* vertex-linked pattern of octahedra. Chains with neither a distinct *cis–trans* nor a *trans–trans* pattern of vertex-linked octahedra, *e.g.* $(Cu(2,2'\text{-dpa})_2MOF_5 \cdot 2H_2O)$ (M = Nb, Ta; dpa = dipyridylamine),[33] may also form a helical structure. Therefore, a closer comparison of metal-oxide/fluoride chains was necessary to search for additional factors that contribute to helical chain formation. Of particular interest to this study was to examine other structural features of a repeating *cis–trans* combination which favor helicity.

Shown in Fig. 4 are small sections of the helical chain in $M(pyz)(H_2O)_2MoO_2F_4$ (M = Zn, Cd) (Fig. 4a) and the zigzag chain in $Cu(pyz)(H_2O)_2TiF_6$ (Fig. 4b), both centered about an MX_6^{2-} anion and extended out to one $M(pyz)_{2/2}(H_2O)_2F_{2/2}$ neighbor on each end. The structural views on the left show each chain projected horizontally, while the views on the right show each chain rotated by 90° and perpendicular to the page. With the exception of the different metal cations, the $M(pyz)_{2/2}(H_2O)_2F_{2/2}$ fragments in both chains are virtually identical to each other, with the same numbers and types of ligands. The $M(pyz)(H_2O)_2MoO_2F_4$ (M = Zn, Cd) chain, however, contains the *cis*-directing $MoO_2F_4^{2-}$ while the $Cu(pyz)(H_2O)_2TiF_6$ chain contains the *trans*-directing TiF_6^{2-}. Furthermore, each individual chain in both structures bonds to six symmetry-equivalent neighboring chains through two covalent M-pyrazine bridges and through four hydrogen bonds to coordinated H_2O molecules. Despite these similarities, the *cis–trans* pattern (Fig. 4a) leads to helical chains, while the *trans–trans* pattern (Fig. 4b) does not.

The ability to control chain structures formed by vertex-linked octahedra requires consideration of both local and extended interactions. The octahedral species MOF_5^{2-} (M = Nb, Ta) and $MO_2F_4^{2-}$ (M = Mo, W) are all polar. As such, they have point group symmetries as shown at the top left of Fig. 5. These asymmetrical anions have non-spherical charge distributions owing to their inherently distorted M–O bonds. These electrostatic potentials result in either a *cis–trans* or *trans–trans* coordination pattern.[31] One example of a *trans*-directing anion is $NbOF_5^{2-}$. The electrostatic potential contour map of this anion (see Fig. 6) illustrates the region of significant charge density localized on the oxide ion. Furthermore, the fluoride ion *trans* to the oxide exhibits a higher electostatic potential than the other four fluoride ions. Hence, the combination of $NbOF_5^{2-}$ anionic units with

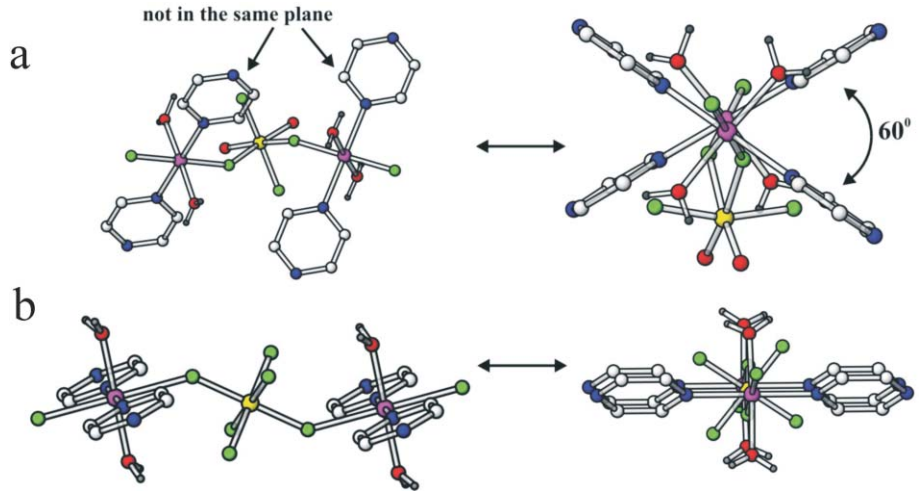

Fig. 4 Comparison of the *cis–trans* chains in $Zn(pyz)(H_2O)_2MoO_2F_4$ (a) and the *trans–trans* chains in $Cu(pyz)(H_2O)_2TiF_6$ (b), aligned horizontally (left) and perpendicular to the page (right).

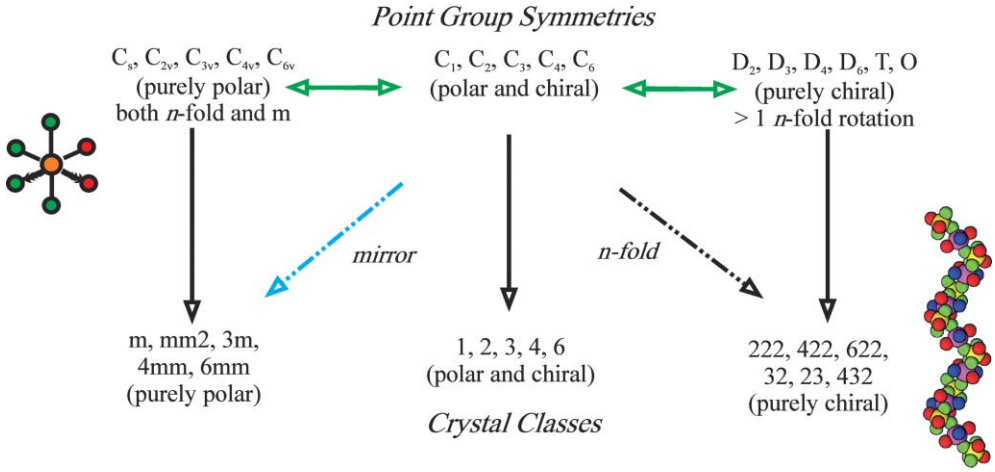

Fig. 5 The top half indicates the point group symmetries that are possible for noncentrosymmetric single packing units. The bottom half indicates the crystal classes possible for a three-dimensional solid comprised of the single units. The blue dashed arrow represents the intracluster symmetry change present with a mirror plane. The black dashed arrow shows the *n*-fold symmetry seen when both enantiomers pack together. Other noncentrosymmetric space groups not represented in the figure are $\bar{4}(S_4)$, $\bar{4}2m(D_{2d})$, $\bar{6}(C_{3h})$, $\bar{4}3m(T_d)$, and $\bar{6}2m(D_{3h})$.

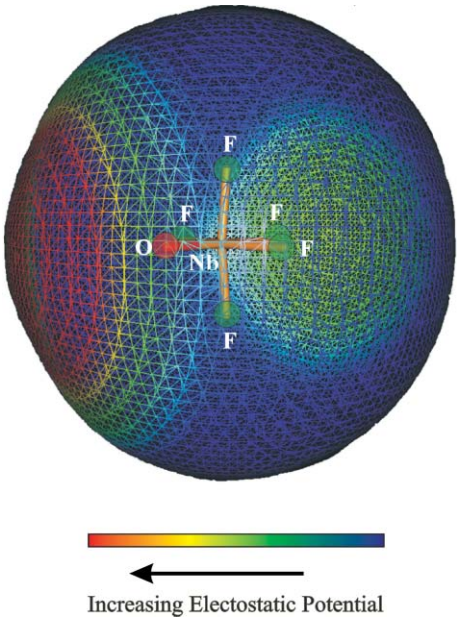

Fig. 6 Geometry optimized $NbOF_5^{2-}$ anion showing the electrostatic potential contour map of the anion. Red denotes the areas of highest electrostatic potential, while blue denotes areas of lowest electrostatic potential.

trans-coordinating cationic units results in a *trans–trans* linear chain structure.

In contrast, the local bonding environment of the $MoO_2F_4^{2-}$ polyhedra includes two *cis*-oxygen positions and four fluorine positions. The molybdenum atom is displaced from the center toward the two *cis*-oxygen positions, resulting in a distorted octahedron with C_{2v} symmetry. The $MoO_2F_4^{2-}$ anion is an example of a *cis*-directing ligand, as it coordinates through the two fluoride vertices that are *trans* to the two *cis*-oxide vertices. In a previous paper, we noted that $M(pyz)(H_2O)_2MoO_2F_4$ (M = Zn, Cd) chains crystallized in a helical structure.[18] The *cis*-directing $MoO_2F_4^{2-}$ polyhedra serve as ''turning'' points that enhance the helical twist of the chains.

An advantage of the helical twist in $M(pyz)(H_2O)_2MoO_2F_4$ (M = Zn, Cd) chains is demonstrated by the reduced steric interactions between the pyrazine ligands that are separated from each other by one repeat unit (upper and lower left of Fig. 4). In the *cis–trans* coordination pattern, the pyrazine ligands from one $M(pyz)_2(H_2O)_2^{2+}$ (M = Zn, Cd) fragment to the next are twisted by *ca.* 60° (right side of Fig. 4a), while the pyrazine ligands for the *trans–trans* chain are in the same plane (right side of Fig. 4b). A hypothetical rotation of the *cis–trans* chain would result in an approximate three-fold decrease in space between the closest carbons in the pyrazine ligands, as shown in Fig. 7. However, in the *trans–trans* chain, no such steric interactions exist as the pyrazine groups are well

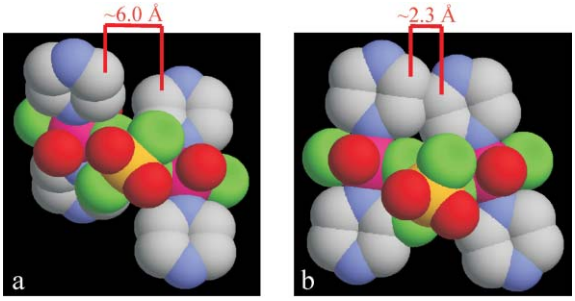

Fig. 7 (a) A space filling model of the *cis–trans* chains in M(pyz)-$(H_2O)_2MoO_2F_4$ (M = Zn, Cd). (b) A space filling model of a hypothetical 60° rotation of the pyrazine ligands highlighting the orbital interaction that would occur in such an arrangement. The figure was generated using the HARLEM (Hamiltonian for response properties of large molecules) suite of programs.[34]

separated and oriented in the same plane. A chain that has neither a distinct *cis–trans* nor a *trans–trans* coordination pattern may twist into a helical conformation when bulky ligand substituents reside in different planes from each other, as was reported for $Cu(2,2'\text{-dpa})_2MOF_5{\cdot}2H_2O$ (M = Nb, Ta; dpa = dipyridylamine).[33]

Pyrazine ligands have important roles in the structures of $Cu(pyz)(H_2O)_2TiF_6$ and $M(pyz)(H_2O)_2MoO_2F_4$ (M = Zn, Cd). As discussed above, the minimization of steric repulsions between pyrazine ligands is an important factor in helix formation, particularly when pyrazine groups serve as linkers between chains. In $Cu(pyz)(H_2O)_2TiF_6$, the pyrazine molecules link zigzag chains to create two-dimensional square nets (Fig. 3). This net motif has two coordinated water molecules to copper directed above and below the 2D plane. Two-dimensional square nets stack in an offset arrangement with hydrogen bonds to fluoride ions (OH···F) on adjacent nets. These hydrogen bonds connect the nets in the third dimension. The chains in $M(pyz)(H_2O)_2MoO_2F_4$ (M = Zn, Cd) are also influenced by M–pyz–M linkages. Because the pyrazine linker is *ca.* 2.8 Å in length, these linked helices are exclusively right- or left-handed in a single crystal domain.[15] The interrelationships between the chirality and/or polarity of local point group symmetries and crystal class symmetries are presented in Fig. 5. The example of $M(pyz)(H_2O)_2MoO_2F_4$ (M = Zn, Cd) clearly demonstrates that the asymmetric and polar $MoO_2F_4^{2-}$ ion (polar point group) can be incorporated into a helix, which in turn packs in a chiral space group. Fig. 5 also illustrates that chiral and polar species can be incorporated into structures belonging to space groups that are exclusively polar, polar and chiral, or only chiral.

Conclusions

The *trans–trans* and *cis–trans* coordination patterns, which have been revealed by comparing related metal-oxide/fluoride phases, demonstrate that the chain motif can be varied from linear to zigzag to helical. Linear chains result when cationic octahedra, which have four equatorial bonds to identical organic ligands, are bonded to *trans*-directing anions in a *trans–trans* vertex-linked pattern. When two of the four equatorial ligands are substituted by water molecules, a bend in the linear chain is observed. These modifications result in a transformation of a linear to zigzag chain and are illustrated in Fig. 1. Fig. 1 also highlights the progression from a zigzag chain to a helical structure when a *trans*-directing anion is replaced by a *cis*-directing anion. This study, which includes a series of related compounds, demonstrates that *trans–trans* vertex-linked octahedra will form either a linear or zigzag chain, depending on the number of pyrazine ligands attached to the cation. Helices will form provided a *cis*-directing anion substitutes for the *trans*-directing ion without altering the number of pyrazine ligands around the cation.

Acknowledgements

The authors gratefully acknowledge support from the National Science Foundation (NSF), Solid State Chemistry (Award No. DMR-0312136), and made use of the Central Facilities supported by the MRSEC program of the National Science Foundation (Grant DMR-0076097) at the Materials Research Center of Northwestern University. The authors also gratefully acknowledge Dr Janet E. Kirsch for stimulating conversations and insight during the preparation of this paper.

References

1 A. Gavezzotti, *Acc. Chem. Res.*, 1994, **27**, 309–314.
2 S. C. Abrahams, *Acta Crystallogr.*, 1994, **A50**, 658–685.
3 *International Tables for Crystallography*, D. Reidel Publishing Company, Boston, MA, 1983; vol. A, p. 782.
4 P. S. Halasyamani and K. R. Poeppelmeier, *Chem. Mater.*, 1998, **10**, 2753–2769.
5 J. F. Nye, *Physical Properties of Crystals*, Oxford University Press, New York, 1985.
6 A. J. Doig, *Biophys. Chem.*, 2002, **101**, 281–293.
7 D. G. Flint, J. R. Kumita, O. S. Smart and G. A. Woolley, *Chem. Biol.*, 2002, **9**, 391–397.
8 B. S. Kinnear and M. F. Jarrold, *J. Am. Chem. Soc.*, 2001, **123**, 7907–7908.
9 G. A. Breaux and M. F. Jarrold, *J. Am. Chem. Soc.*, 2003, **125**, 10740–10747.
10 M. R. Bauer, D. L. Pugmire, B. L. Paulsen, R. J. Christie, D. J. Arbogast, C. S. Gallagher, W. V. Raveane, R. M. Nielson, C. R. II Ross, P. Photinos and S. C. Abrahams, *J. App. Crystallogr.*, 2001, **34**(1), 47–54.
11 A. J. Norquist, K. R. Heier, P. S. Halasyamani, C. L. Stern and K. R. Poeppelmeier, *Inorg. Chem.*, 2001, **40**, 2015–2019.
12 P. A. Maggard, T. S. Nault, C. L. Stern and K. R. Poeppelmeier, *J. Solid State Chem.*, 2003, **175**(1), 27–33.
13 Z. Shi, S. Feng, L. Zhang, S. Gao, G. Yang and J. Hua, *Angew. Chem. Int. Ed.*, 2000, **39**(13), 2325–2327.
14 L. Carlucci, G. Ciani, D. M. Proserpio and A. Sironi, *Inorg. Chem.*, 1998, **37**, 5941–5943.
15 P. A. Maggard, C. L. Stern and K. R. Poeppelmeier, *J. Am. Chem. Soc.*, 2001, **123**, 7742–7743.
16 M. E. Welk, A. J. Norquist, C. L. Stern and K. R. Poeppelmeier, *Inorg. Chem.*, 2001, **40**, 5479–5480.
17 K. R. Heier, A. J. Norquist, C. G. Wilson, C. L. Stern and K. R. Poeppelmeier, *Inorg. Chem.*, 1998, **37**, 76–80.
18 P. A. Maggard, A. L. Kopf, C. L. Stern and K. R. Poeppelmeier, *Inorg. Chem.*, 2002, **41**, 4852–4858.
19 A. F. Wells, *Structural Inorganic Chemistry*, Oxford University Press, New York, 5th edn., 1984, p. 203.
20 W. T. A. Harrison, T. M. Nenoff, T. E. Gier and G. D. Stucky, *Inorg. Chem.*, 1993, **32**, 2437–2441.
21 $Cu(C_4H_4N_2)(H_2O)_2TiF_6$, Fw = 341.56, a = 12.703(2) Å, b = 6.879(1) Å, c = 10.819(2) Å, β = 95.426(2)°, V = 941.1(2), T = 153(2) K, $C2/c$ (No. 15), Z = 4, μ (Mo Kα) = 3.190 mm^{-1}, reflections (total) = 4141, final $R1$(obs) = 0.034, final $wR2$ (obs) = 0.086.
22 SAINTPLUS Bruker, AXS, Inc., Madison, WI, 1997.
23 G. M. Sheldrick, SHELXTL Programs, Version 5.1 Bruker AXS, Inc., Madison, WI, 1998.
24 A. L. Spek, PLATON, Utrecht University, Utrecht, The Netherlands, 2001.
25 J. M. Lockhart, R. L. Fagaly, L. W. Lombardo and B. Muhlfelder, *Physica B*, 1990, **165**, 147–148.
26 P. S. Halasyamani, K. R. Heier, C. L. Stern and K. R. Poeppelmeier, *Acta Crystallogr.*, 1997, **C53**, 1240–1244.
27 K. Nakamoto, *Infrared and Raman Spectra of Inorganic and Coordination Compounds, Part A*, John Wiley & Sons, New York, 1997.
28 C. J. Pouchert, *The Aldrich Library of FT-IR Spectra*, Aldrich Chemical Co., Milwaukee, WI, 1997.
29 R. S. Drago, *Physical Methods for Chemists*, Saunders College Publishing, Orlando, FL, 1992.
30 P. S. Halasyamani, M. J. Willis, C. L. Stern, P. M. Lundquist,

G. K. Wong and K. R. Poeppelmeier, *Inorg. Chem.*, 1996, **35**, 1367–1371.
31 A. J. Norquist, K. R. Heier, C. L. Stern and K. R. Poeppelmeier, *Inorg. Chem.*, 1998, **37**, 6495–6501.
32 I. Trodjman, R. Masse and J. C. Guitel, *Z. Kristallogr.*, 1974, **139**, 103–115.
33 A. J. Norquist, C. L. Stern and K. R. Poeppelmeier, *Inorg. Chem.*, 1999, **38**, 3448–3449.
34 I. Kurnikov, Welcome to HARLEM home, http://www.kurnikov.org/harlem_main.html (accessed April 2004), freeware download.